Universal Scaling and Design Rules of Hydrogen-Induced Optical Properties in Pd and Pd-Alloy Nanoparticles

Citation for the original published paper (version of record):
Nugroho, F., Darmadi, I., Zhdanov, V. et al (2018). Universal Scaling and Design Rules of Hydrogen-Induced Optical Properties in Pd and Pd-Alloy Nanoparticles. ACS Nano, 12(10): 9903-9912. http://dx.doi.org/10.1021/acsnano.8b02835

(article starts on next page)

ACS NANO

Cite This: ACS Nano 2018, 12, 9903−9912

www.acsnano.org

ARTICLE

Universal Scaling and Design Rules of Hydrogen-Induced Optical Properties in Pd and Pd-Alloy Nanoparticles

Ferry Anggoro Ardy Nugroho,*,† Iwan Darmadi,† Vladimir P. Zhdanov,†,‡ and Christoph Langhammer*,†

†Department of Physics, Chalmers University of Technology, 412 96 Göteborg, Sweden

‡Boreskov Institute of Catalysis, Russian Academy of Sciences, Novosibirsk 630090, Russia

Supporting Information

ABSTRACT: Hydride-forming metal nanoparticles sustaining localized surface plasmon resonance have emerged as prototypical material to study the fundamentals of hydrogen-induced phase transformations. They have also been proposed as signal transducers in next-generation hydrogen sensors. However, despite high current interest in hydrogen sorption by nanomaterials in general and such sensors in particular, the correlations between nanoparticle size, shape, and composition, the amount of hydrogen absorbed, and the obtained optical response have not been systematically experimentally studied. Focusing on hydrogenated Pd, PdAu- and PdCu-alloy nanoparticles, which are of particular interest in hysteresis-free plasmonic hydrogen sensing, we find that at practically important Au/Pd and Cu/Pd ratios the optical response to hydrogen concentration is linear and, more interestingly, can be described by a single universal linear trend if constructed as a function of the H/Pd ratio, independent of alloy composition. In addition to this correlation, we establish that the amplitude of optical signal change is defined solely by the spectral plasmon resonance position in the non-hydrogenated state for a specific nanoparticle composition. Thus, it can be maximized by red-shifting the LSPR into the NIR spectral range via tailoring the particle size and shape. These findings further establish plasmonic sensing as an effective tool for studying metal−hydrogen interactions in nanoparticles of complex chemical composition. They also represent universal design rules for metal-hydride-based plasmonic hydrogen sensors, and our theoretical analysis predicts that they are applicable not only to the H/Pd/Au or H/Pd/Cu system investigated here but also to other H/Pd/Metal combinations.

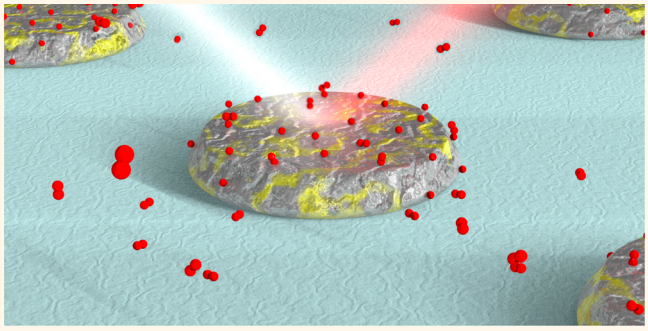

KEYWORDS: *optical response, hydrogen sorption, nanoparticles, palladium alloys, hydrogen sensors, universal scaling, design rules*

The localized surface plasmon resonance (LSPR)[1] has established itself as a basis for important experimental tools to unravel the fundamentals of nanosizing effects in the hydrogenation of metallic nanoparticles both at the ensemble and single-nanoparticle level,[2−7] as well as a promising platform for application in next-generation hydrogen detection devices.[8−14] At the heart of nanoplasmonic optical hydrogen sensors are metallic nanoparticles that absorb hydrogen in solid solution and undergo phase transformation into metal hydride upon hydrogen exposure at higher partial pressures. Consequently, the LSPR signal changes dynamically along the (de)hydrogenation process.[8] For Pd nanoparticles, the prototype material used in the field, a linear correlation between LSPR peak shift, $\Delta\lambda_{peak}$, and the corresponding hydrogen concentration in the metal has been established experimentally by using a quartz crystal microbalance (QCM)[3] and theoretically by first-principle calculations.[15] However, at a more general level involving other materials than Pd, such correlation has neither ever been experimentally verified in general nor, for example, in the context of "active plasmonics".[13,16,17] Until very recently for Hf,[18] also in the so-called optical hydrogenography method of thin films[19] widely used for the screening of complex hydrogen storage materials,[20−22] switchable mirrors,[23,24] and also for optical hydrogen detection,[25−27] the change in the transmission/reflection properties upon hydrogenation has been generally assumed to be linearly related to hydrogen concentration in the film based on the Beer−Lambert law. For Pd-based

Received: April 16, 2018
Accepted: August 29, 2018
Published: August 29, 2018

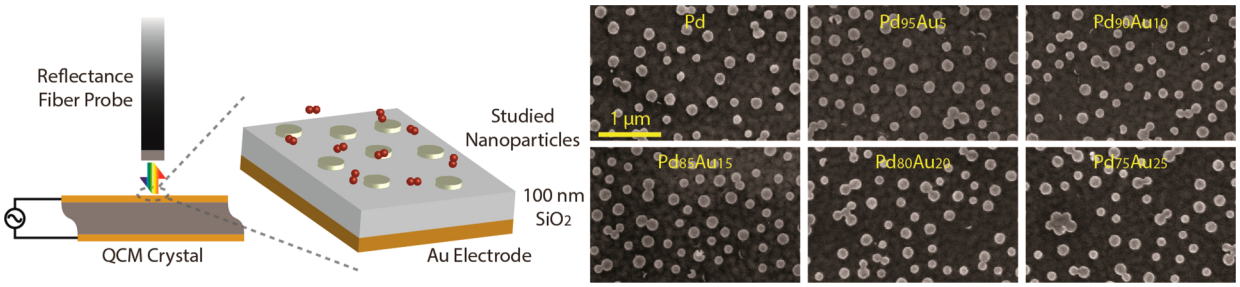

Figure 1. Integrated QCM and LSPR. (left) Schematic depiction of the combined QCM and optical readout setup, where the latter is implemented in reflection mode *via* a fiber optic reflectance probe connected to a white light source and a fixed-grating spectrometer. To minimize coupling of the LSPR modes in the investigated nanoparticles with the Au electrode of the QCM crystal, a 100 nm thick SiO_2 spacer layer is grown on the QCM electrode, onto which the nanoparticles subsequently are fabricated. (right) SEM micrographs of PdAu alloy nanoparticles with different compositions ($Pd_{100-x}Au_x$, x = 0, 5, 10, 15, 20, and 25 at. %) but identical dimension (190 nm diameter and 25 nm thickness) fabricated on QCM crystals.

systems in focus here, the only attempt to correlate these two properties was done based on different types of samples (thin film and bulk) studied by different groups in separate measurements.[28] To further advance the performance of optical hydrogen sensors and other systems, as well as the understanding of the corresponding material physics that govern the optical properties of metal nanosystems interacting with hydrogen, it is therefore of fundamental importance to experimentally unambiguously correlate optical property changes of state-of-the-art materials and nanostructures with corresponding changes of the hydrogen concentration inside them, and to evaluate to which extent the widely *assumed* linear correlations are generically valid and depend on nanostructure size, shape, and composition. Furthermore, plasmonic sensing as a tool to scrutinize the materials science of the hydrogenation process in individual *neat* Pd nanoparticles using either electron energy loss spectroscopy (EELS)[7,29,30] or plasmonic nanospectroscopy[5,6,9,31,32] has demonstrated exceptional potential. Hence, establishing a more general understanding of the nature of the scaling between plasmonic response and hydrogen concentration in nanomaterials will enable the use of these powerful single nanoparticle experimental techniques also on more complex materials to, in turn, generate deep insights in the fundamental properties of these systems at the individual nanoparticle level.

To address these points, we have established a robust protocol for the *simultaneous* quantification of hydrogen concentration in nanoparticles of different size and chemical composition and of their optical response. This becomes possible by using a combined LSPR-QCM setup comprised exclusively of commercially available components (in contrast to our earlier custom-built electrodeless solution[33]), which also is applicable to thin film systems (in the earlier QCM-based quantification of hydrogen uptake by thin films,[34] the corresponding optical response was not studied). As the system of interest to reveal the correlation between hydrogen content and optical response, we chose the PdAu and PdCu alloy family, because, compared to neat Pd, introducing other metallic elements to a hydride-forming substrate, *e.g.*, PdAu,[27,35] PdCu,[36,37] and PdAg,[38,39] enables modification of its thermodynamic and kinetic properties as well as improves the resistance to poisoning by species like CO and SO_x, which is critical for hydrogen sensor applications. Specifically, as we have shown for the PdAu alloy nanoparticle system,[13,40] upon hydrogen absorption and desorption the inherent hysteresis, as well as the two-phase coexistence plateau characteristic for neat Pd, vanishes at 25 at. % Au, increasing both sensor bandwidth and accuracy. In addition, the random alloy formation of Pd with Au improves the response time of a sensor based on these materials due to faster kinetics.[13,14,41,42]

As the main results of our present study, first, we find a linear correlation of the characteristic optical readout parameters LSPR peak position shift, $\Delta\lambda_{peak}$, and change of LSPR peak full width at half-maximum, Δfwhm, with hydrogen concentration in the PdAu alloy nanoparticles at hand. Surprisingly, the linear scaling represented as a function of the H/Pd ratio is *independent* of the Au content in the alloy for a given nanoparticle dimension, implying an alloy-composition-independent optical response per absorbed hydrogen atom, in good agreement with a phenomenological theoretical analysis. Second, we find a nanoparticle volume- and shape-independent linear scaling of the magnitude of $\Delta\lambda_{peak}$ to hydrogen with the spectral peak position of the nanoparticles in the metallic state. In other words, we unravel a generic and material-independent design rule for nanoplasmonic hydrogen sensors, which states that higher sensitivity can be achieved by shifting the LSPR to longer wavelength by tailoring the geometry of the used nanoparticles.

RESULTS AND DISCUSSION

To accommodate measurements of the Pd alloy nanoparticle optical response directly on a QCM crystal, we rely on the fact that the Au electrode of the crystal can serve as a mirror (it is optically opaque) and thus enables efficient reflectivity measurements. As shown schematically in Figure 1, however, a *thick* dielectric spacer must be grown to control coupling between the plasmonic entities and the mirror in order to assess the intrinsic response of the nanoparticles.[43,44] However, we also note that, if desired, the sensitivity of the system can be tuned by varying, *e.g.*, the spacer dielectric thickness and/or material.[45,46] Here we deposited 100 nm of dense SiO_2 by PECVD on a commercial SC-cut 10 MHz QCM crystal with standard Au electrode (*i.e.*, no custom-made crystals are necessary as used in earlier approaches combining LSPR with QCM[33,47,48]), onto which Pd and PdAu alloy nanoparticles (in the form of nanodisks) with different composition ($Pd_{100-x}Au_x$, x = 0, 5, 10, 15, 20, and 25 at. %, diameter and height of 190 and 25 nm, respectively) were fabricated by hole−mask colloidal lithography[49] following our established homogeneous-alloy-formation approach.[13,40] The nanoparticles occupy *ca.* 16−19% of the surface area of the QCM crystal (Figure 1 and Table S1 in the Supporting Information (SI)). The

DOI: 10.1021/acsnano.8b02835
ACS Nano 2018, 12, 9903−9912

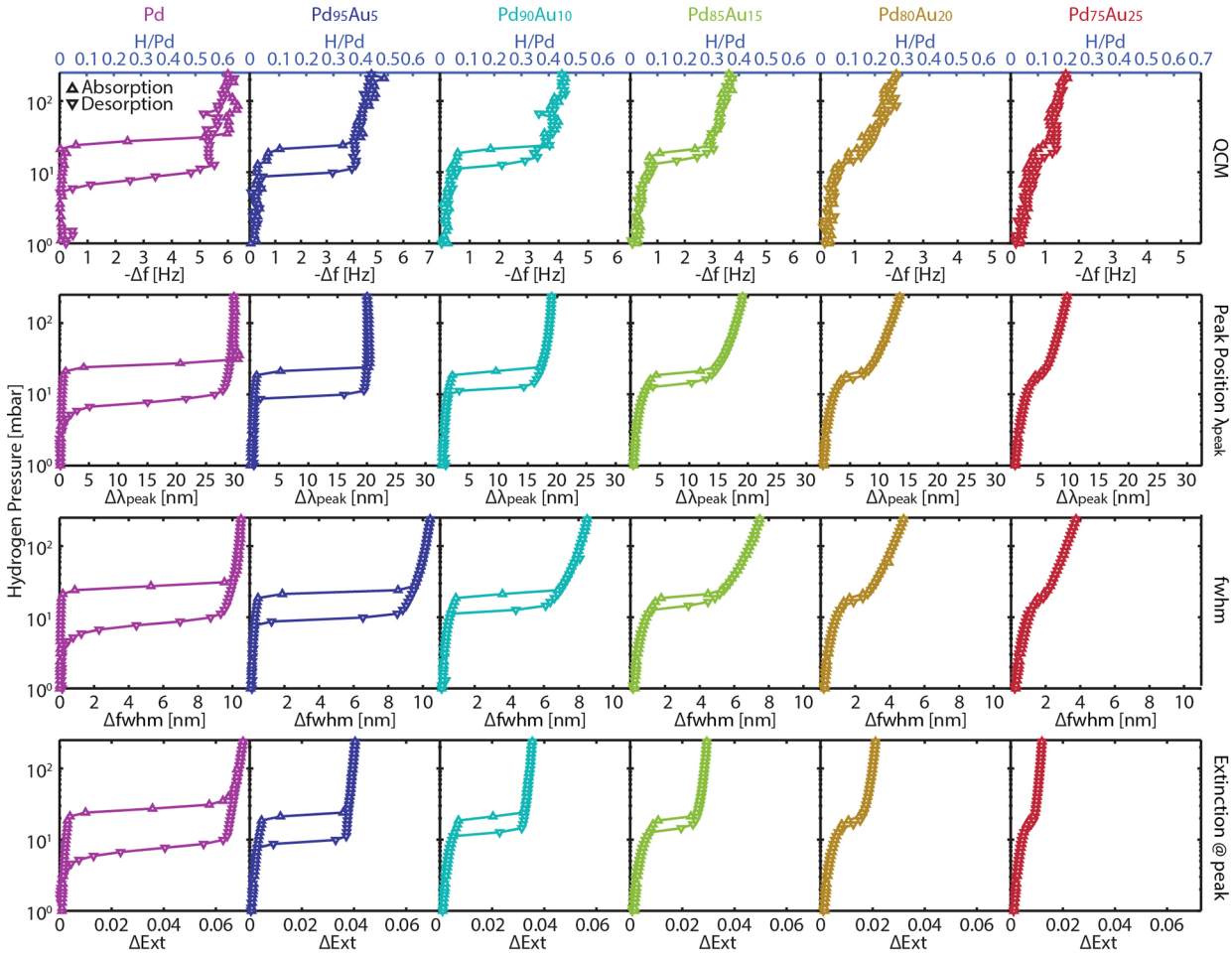

Figure 2. Simultaneously measured gravimetric (QCM) and optical (LSPR) hydrogen absorption and desorption isotherms in Pd and PdAu alloy nanoparticles (mean diameter and height of 190 and 25 nm, respectively) of five different compositions measured at 303 K. The hydrogen concentration in the nanoparticles (expressed as the hydrogen to palladium atom ratio, H/Pd) as a function of applied hydrogen partial pressure in the gas phase, is calculated from the QCM data *via* the measured frequency shift of the QCM crystal upon hydrogenation and the Sauerbrey equation (details are described in the SI). Shifts/changes in LSPR peak spectral position $\Delta\lambda_{peak}$, full width at half-maximum (Δfwhm), and extinction at peak (ΔExt) are used as descriptors of the optical property changes of the alloy nanoparticles during hydrogenation. The upward and downward triangles denote the hydrogen absorption and desorption branches of the isotherm, respectively.

extinction spectra collected in a reflection configuration upon illumination at normal incidence exhibit a broad peak due to the lossy characteristics of Pd at visible frequencies[40] (SI, Figure S11).

The hydrogen sorption measurements were conducted in flow mode by connecting a QCM window module to a set of mass flow controllers to regulate the partial pressure of H_2 in Ar carrier gas. Using a fiber optic reflectance probe positioned above the QCM crystal decorated with the PdAu nanoparticles (Figure 1, and details of the setup are presented in the SI), both the QCM frequency shift related to the change in mass (*via* the Sauerbrey equation[50]) and the corresponding optical LSPR readout due to the change of optical properties of the nanoparticles can be measured simultaneously and thus directly correlated as a function of H_2 partial pressure.

One of the main challenges in this approach is that QCM measurements suffer from drift over time.[51] This is a particular problem in experiments where the hydrogen partial pressure is gradually changed because the overall frequency shift due to hydrogen sorption is very small due to the low mass of H. To overcome this problem and obtain highly reproducible and accurate measurements not plagued by drift effects, we instead executed a series of hydrogen pulses at each measured partial pressure. In this way, for each pressure step, a clear baseline is established and drift becomes irrelevant so that we can unambiguously assign frequency shifts to the corresponding change in the gas partial pressure (see SI for details). Consequently, completely reversible pressure−composition isotherms can be obtained.

On the basis of this procedure, we measured at 303 K gravimetrically (QCM) and optically (LSPR) the hydrogen absorption and desorption isotherms for the fabricated Pd and PdAu alloy nanoparticles with different compositions (Figure 2). For the QCM experiments, we plot the obtained data by translating the measured QCM-crystal frequency shifts to the corresponding hydrogen concentration in the nanoparticles (hereafter expressed as hydrogen to palladium atom ratio, H/Pd), as obtained from careful analysis of the surface coverage of the nanoparticles for each individual sample (see SI for detailed analysis and derivation). For the LSPR measurements, we plot the isotherms based on three readout parameters, $\Delta\lambda_{peak}$, Δfwhm, and ΔExt. Immediately, we noticed the striking similarity between the QCM and $\Delta\lambda_{peak}$ and Δfwhm optical

DOI: 10.1021/acsnano.8b02835
ACS Nano 2018, 12, 9903−9912

isotherms. We also notice the slightly different appearance of the isotherms obtained from the ΔExt readout.

A common feature for all four series of isotherms is that, with increasing Au content in the Pd and the PdAu alloy, the hysteresis between absorption and desorption gradually shrinks, shifts to the left, and eventually disappears for $Pd_{75}Au_{25}$. Similarly, a narrowing of the α- and β-phase coexistence region at the characteristic plateau is observed irrespective of the used readout parameter. These observations are in excellent agreement with previous studies on nanoparticles[13] and (thin) films[27,35,42] of similar alloys and thus corroborate that the nanoparticles investigated here are homogeneously alloyed. Furthermore, we find that in the α-phase (up to ~20 mbar) the hydrogen solubility increases with increasing Au content in the alloy (SI, Figure S7).

The hydrogen concentration at 250 mbar H_2 partial pressure, again expressed as H/Pd ratio, is plotted as a function of the Au content in the alloy nanoparticles (Figure 3). For pure Pd, a H/Pd ratio of 0.65 is found, in excellent agreement with bulk and thin film values.[52,53] The H/Pd ratio then decreases linearly with increasing Au content until it reaches 0.22 for the alloy containing 25 at % Au. This trend is quantitatively in excellent agreement with results reported for bulk systems[37,42,54] and can be rationalized by a diminishing number of Pd atoms neighboring the octrahedral interstitial sites occupied by hydrogen[37] (the interaction of hydrogen atoms with Au or, *e.g.*, Ag and Cu, is sizable but weaker than with Pd[55]). The similarity with bulk data is expected because our nanoparticles are in the size regime where the thermodynamic properties are comparable to those of bulk systems.[5,7,56] At first sight, the qualitative trend of the hydrogen concentration as a function of Au content in the alloy nanoparticles is also directly reflected in the corresponding change of optical properties, that is, their plasmonic response readout parameters (*cf.*, Figure 2), which become smaller as the Au concentration is increased.

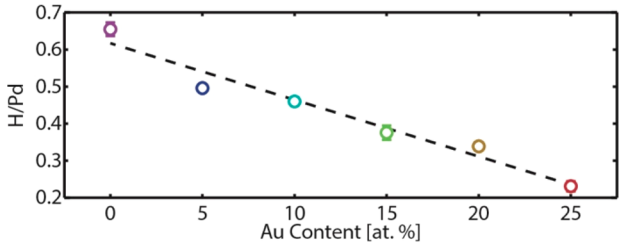

Figure 3. Experimentally determined (QCM) relative hydrogen concentrations in Pd and PdAu alloy nanoparticles with different Au content at 250 mbar hydrogen partial pressure, measured at 303 K. The relative hydrogen concentration, expressed as hydrogen to palladium atom ratio, H/Pd, for each system (*i.e.*, the Au atoms are subtracted), decreases linearly as the Au content in the alloy is increased. The data points are averaged from at least three measurements and, in most of the cases, the error bars are smaller than the symbols. The dashed line is a guide to the eye.

In the next step, we directly correlate the optical property changes of the alloy nanoparticles upon variation of hydrogen partial pressure with the corresponding change of hydrogen concentration in the nanoparticles by plotting the two parameters as a function of each other. Figure 4a–f shows the corresponding results for the $\Delta\lambda_{peak}$ readout for all considered alloy systems (see SI for identical figures using Δfwhm and ΔExt). We find linear correlations for all systems with root-mean-square errors (RMSE) ≤ 0.030 H/Pd. For the pure Pd nanoparticles, this result corroborates previous experimental[3] and theoretical[15] studies. For alloy nanoparticles, they facilitate a direct comparison of the optical response toward hydrogen exposure and the corresponding amount of hydrogen dissolved in alloy systems with different compositions. Fascinatingly, all systems exhibit basically identical scaling factors, *i.e.*, slope of the linear regression, of ~0.020 (H/Pd)/nm. To further verify this alloy-composition-independent scaling, we plot the $\Delta\lambda_{peak}$ signals from all the samples in a single graph (Figure 4g). Evidently, all the data fall onto a single trend.

This universal scaling factor has a number of consequences. First, it demonstrates that the absolute $\Delta\lambda_{peak}$ value is

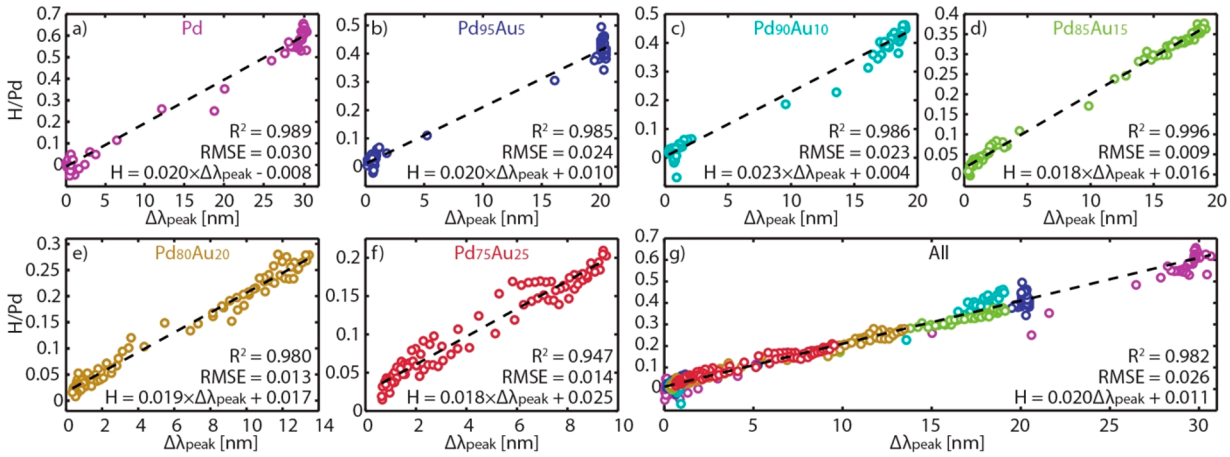

Figure 4. Correlation between the optical readout parameter $\Delta\lambda_{peak}$ and relative hydrogen concentration in Pd and PdAu alloy nanoparticles of fixed size but with different composition, (a) Pd, (b) $Pd_{95}Au_5$, (c) $Pd_{90}Au_{10}$, (d) $Pd_{85}Au_{15}$, (e) $Pd_{80}Au_{20}$, and (f) $Pd_{75}Au_{25}$. Linear regression (dashed lines) is applied to describe the $\Delta\lambda_{peak}$–hydrogen concentration relation and shown together with corresponding R^2 and root-mean-square error (RMSE) values. Note how all the systems exhibit similar slopes and thus scaling with the hydrogen concentration in the nanoparticles expressed as H/Pd. This becomes particularly clear in the master plot (g) where data for the different alloy compositions are all plotted together.

DOI: 10.1021/acsnano.8b02835
ACS Nano 2018, 12, 9903−9912

determined solely by the relative hydrogen concentration (*i.e.*, H/Pd) in the system, regardless of the alloy composition. Second, it means that one can use $\Delta\lambda_{peak}$ to extract the hydrogen concentration in the nanoparticle from any alloy composition by simply calibrating it to the $\Delta\lambda_{peak}$ of a fully hydrided Pd nanoparticle reference (with identical particle dimensions, see below), which will always have a very well-documented H/Pd = 0.67 at 1 bar of hydrogen partial pressure, provided it is larger than *ca.* 10 nm.[52,53] Notably, the same universal scaling also holds for Δfwhm (SI, Figure S8), whereas for ΔExt, the α-phase and β-phase regions exhibit slightly different scaling factors (SI, Figure S8 and S10, respectively).

To understand the physics of the $\Delta\lambda_{peak}$−hydrogen concentration scaling factor universality in PdAu alloys with different compositions, we execute a phenomenological theoretical analysis. Concerning this aspect of our work, we highlight that a more conventional analysis might, in principle, be based on the use of the dielectric function of the systems at hand for accurate calculation of the optical response of nanoparticles using analytical or numerical methods. In our case, however, such calculations are not possible due to the lack of the necessary input in the literature in the form of accurate dielectric functions for PdAu alloys in both their pure and hydrogenated state. As an approximation, one could also consider to employ, *e.g.*, the Drude theory of electrons in metals for the description of the dielectric function of the alloy. This approach, however, fails to capture the key features observed in our experiments (as we discuss in detail in section 11 of the SI), *i.e.*, the formation of the joint pool of electrons with its own Fermi energy is not sufficient in order to explain our results.

To start our phenomenological analysis, we recall that near the LSPR peak position, λ_{peak}, the strong interaction of Pd nanoparticles with light is caused by the excitation of LSPR and by interband transitions from occupied Pd d-bands to unoccupied sp states (see, *e.g.*, the DFT calculations[57]). To this end, hydrogen absorption in Pd results in the appearance of a split-off band below −6 eV (at about −8 eV).[57,58] This new well-separated band contains H 1s states and Pd 5sp and 4d states shifted downward. Because of this shift, there is a band narrowing including Pd 5sp and 4d states above −6 eV. The energy of the electrons in the split-off band (*i.e.*, electrons bound to the absorbed protons) is very low, *i.e.*, significantly below the Fermi level. Thus, their *direct* contribution to light absorption near λ_{peak} is negligible. Their "*indirect*" and sizable contribution to λ_{peak} is related to the modification of the density of states responsible for the light absorption in the hydrogenated system. In particular, increasing the H concentration results in a reduction of the density of states at the Fermi level and in an increasing importance of interband transitions.[57] This, in turn, gives rise to a spectral red-shift of λ_{peak}, as observed in many experimental studies.[1]

With the general background of the problem at hand outlined above, λ_{peak} of a PdAu alloy nanoparticle can phenomenologically be represented as a function of four parameters,

$$\lambda_{peak} = \varphi(\eta_{Pd}, \eta_{Au}, N_{Pd}, N_{Au}) \quad (1)$$

where N_{Pd} and N_{Au} are the number of Pd and Au atoms in the nanoparticle, respectively, and the parameters η_{Pd} and η_{Au} account for the indirect effect of H on the electronic states of Pd and Au. The latter two parameters depend on the number of H atoms, N_H, and also on N_{Pd} and N_{Au}. This dependence is determined by the specifics of the spatial distribution of H, Pd, and Au atoms in the alloy nanoparticle. During hydrogen absorption in the PdAu alloy, for energetic reasons,[59] the H atoms are expected to be primarily localized in contact with Pd atoms, provided the fraction of Au atoms is small enough (*i.e.*, ≤ *ca.* 0.30 at. %).[42,60] Mathematically, this means that η_{Au} can be neglected, while η_{Pd} depends on the average number of H atoms which are nearest-neighbor to a Pd atom, *i.e.*, N_H/N_{Pd}. Taking into account that the effect of H on λ_{peak} is relatively small, we can expand η_{Pd} and then φ with respect to N_H/N_{Pd} and take into account only the linear term (this procedure is valid provided the ratio N_H/N_{Pd} is not large). This procedure yields

$$\Delta\lambda_{peak} = \phi(N_{Pd}, N_{Au})N_H/N_{Pd} \quad (2)$$

where $\phi(N_{Pd}, N_{Au})$ is a function which can be expressed via the derivative of $\varphi(\eta_{Pd}, \eta_{Au}, N_{Pd}, N_{Au})$ with respect to η_{Pd}. To this end, the scaling of the dependence of ϕ on N_{Pd} and N_{Au} will be the same as that of φ $(\eta_{Pd}, \eta_{Au}, N_{Pd}, N_{Au})$ provided that η_{Pd} and η_{Au} are negligible (*i.e.*, in the absence of hydrogen). Thus, under the present condition of a low fraction of Au atoms in the alloy (*i.e.*, ≤ *ca.* 25 at. %), the dependence of φ on N_{Pd} and N_{Au} is weak, as manifested in the experimentally observed small change in λ_{peak} as a function of Au content in the PdAu alloy particles in the non-hydrogenated state (SI, Figure S11). Thus, in this regime $\phi(N_{Pd}, N_{Au})$ can be considered to be constant to a first approximation, and accordingly $\Delta\lambda_{peak}$ upon hydrogen sorption is proportional to N_H/N_{Pd}, as observed in the experiments. The localization of H atoms primarily near Pd atoms is also the reason why, with increasing the Au content, the effect of H absorption on λ_{peak} and fwhm is slightly stronger than on extinction, Ext (Figure 2 and SI, Figure S9), because λ_{peak} (and fwhm) is more related to the Pd host.

At this point, it is important to mention that our theoretical analysis also implies that the $\Delta\lambda_{peak}$−hydrogen concentration scaling factor universality holds true for other alloyants than Au, under the condition that they are weakly interacting with hydrogen. To prove this hypothesis, we carried out a similar set of experiments for PdCu alloy nanoparticles covering the same alloyant concentration range from 0−25 at. % (SI, Figure S14). We chose PdCu to serve as a contrasting complement to PdAu in the sense that it contracts, rather than expands, the Pd lattice (*i.e.*, a_{Pd} = 3.89 Å, a_{Au} = 4.08 Å, a_{Cu} = 3.61 Å). Thermodynamically, this translates into a higher energy barrier for the hydride formation phase transition and, hence, hydrogenation occurs at higher pressure than for pure Pd.[36,61] As anticipated from our theoretical treatment and despite the opposite effect on the host lattice compared to PdAu, the universal and alloy composition independent scaling also applies to PdCu system (SI, Figure S16).

Having established this universal scaling of the LSPR readout for the Pd alloy nanoparticles of *fixed size*, we set out to investigate the particle size dependence by again focusing on the PdAu system. This is motivated by the fact that in traditional bulk refractive index plasmonic sensing, sensitivity directly correlates with particle size and shape through the size- and shape-dependence of the LSPR wavelength.[62,63] For this purpose, we compared two new sets of Pd and $Pd_{75}Au_{25}$ nanoparticles, this time fabricated on glass substrates (*i.e.*, no QCM measurements), for which we varied the diameter in the range of 140−210 nm and the height between 20−46 nm. Among these, we designed three samples

DOI: 10.1021/acsnano.8b02835
ACS Nano 2018, 12, 9903−9912

for each of the two compositions such that they have almost identical volume despite different diameters and heights (140 nm × 46 nm, 170 nm × 31 nm, and 190 nm × 25 nm) and thus different LSPR wavelength. In this way, it is possible to determine whether the obtained $\Delta\lambda_{peak}$ depends on the absolute amount of absorbed hydrogen atoms (in this case, a larger particle volume should yield a larger $\Delta\lambda_{peak}$) or if it is dictated by the spectral position of the LSPR, as is the case for the bulk refractive index sensitivity (in this case a red-shifted peak position in the metallic state should yield a larger $\Delta\lambda_{peak}$, irrespective of the particle volume and the total amount of absorbed H atoms).

This analysis summarized in Figure 5 reveals that, indeed, both for the pure Pd and the $Pd_{75}Au_{25}$ case, the $\Delta\lambda_{peak}$ value

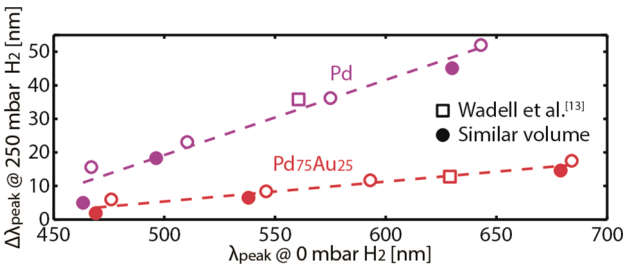

Figure 5. $\Delta\lambda_{peak}$ of a set of Pd (purple) and $Pd_{75}Au25$ (red) samples with different nanodisk dimensions (see main text) upon hydrogenation at 250 mbar at 303 K (corresponding to H/Pd of 0.65 and 0.22 for Pd and $Pd_{75}Au_{25}$, respectively) plotted as a function of their corresponding LSPR peak position, λ_{peak}, in the non-hydrogenated state. The data were acquired by optical measurements in transmission mode (*i.e.*, no QCM). Clearly, the $\Delta\lambda_{peak}$ values correlate linearly with their corresponding λ_{peak} in the non-hydrogenated state. This observation, along with the large variation of $\Delta\lambda_{peak}$ found for three samples with nanoparticles of similar volume but very different peak positions (filled circles), implies that the scaling factor of the optical response to hydrogen is dictated by the spectral position of the LSPR rather than the absolute amount of absorbed H. The data points depicted as squares are adapted from Wadell *et al.*[13] The dashed lines are guides to the eye. Error bars are on the order of or smaller than the symbol size and thus not explicitly shown.

obtained upon hydrogenation (here plotted at 250 mbar) solely and linearly depends on the spectral position of the LSPR of the nanoparticles in the non-hydrogenated state (*i.e.*, at 0 mbar H_2, see SI, Figure S13) and is *not* dictated by the absolute amount of H atoms in the system. The validity of this relation is further strengthened by including our previous data[13] (squares in the plot), which seamlessly fit into the trend. In other words, the more red-shifted LSPR peak, the higher its sensitivity toward hydrogen and thus the amplitude of the optical response.

To understand this result, it is instructive to look at the raw data that are the basis of the analysis summarized in Figure 5. The corresponding time-evolution of the $\Delta\lambda_{peak}$ signals upon hydrogen absorption and desorption at/from 250 mbar at 303 K for the whole sample series is shown in Figure 6a−g. The data are plotted such that all the $\Delta\lambda_{peak}$ values (left *y*-axes) are *scaled* to the hydrogen concentration of H/Pd = 0.65 for pure Pd (right *y*-axis), as determined above by QCM (*cf.* Figure 3). Clearly, the $\Delta\lambda_{peak}$ values for the $Pd_{75}Au_{25}$ samples with different dimension scaled in this way then all are very similar and in excellent agreement with the hydrogen concentration of H/Pd = 0.22 *independently* obtained above using QCM on only a single set of particle dimensions (*cf.* Figure 3). Furthermore, as shown in Figure 6h, the ratios between the $\Delta\lambda_{peak}$ of corresponding Pd and $Pd_{75}Au_{25}$ samples are all similar, independent of size/volume, and agree excellently with the ratio of the hydrogen concentration in pure Pd and in $Pd_{75}Au_{25}$ (*i.e.*, 0.65/0.22 = 2.95, marked by a dashed line). These results thus imply that the PdAu alloy-composition-independent LSPR-response to hydrogen also prevails in nanostructures with different size/volume, however, with different scaling factors for a given nanoparticle dimension due to different spectral positions of the LSPR (*cf.* Figure 5).

On the basis of these findings, we can now construct universal optical response or "hydrogen sensitivity" (*i.e.*, nm/H/Pd) curves for Pd and PdAu alloy nanoparticles by dividing the obtained $\Delta\lambda_{peak}$ at 250 mbar (*cf.* Figure 5) by their known hydrogen concentration expressed as H/Pd (Figure 7a). These curves reveal a universal linear dependence of the amplitude of the optical response on the spectral position of the LSPR of the nanoparticles in the non-hydrogenated state, with slightly different slopes for the pure Pd and the $Pd_{75}Au_{25}$ alloy. Furthermore, it again becomes apparent that for alloyed particles with similar dimension the amplitude of the response is constant (*e.g.*, see the set of Pd and $Pd_{75}Au_{25}$ data pairs, connected with gray dashed lines). This is further exemplified by including a set of data adapted from Wadell et al.[13] (squares), in which all alloy compositions studied have essentially the same response amplitude.

To further evaluate the universality of the identified correlations, as the last step of our analysis, we have collected from the literature the available data for the optical LSPR response of Pd-based nanoparticles measured at similar conditions as in the present study. These data include nanostructures with various dimensions and also two different shapes, *i.e.*, nanodisks[3,8] and nanorings.[3,64] Plotting their sensitivities together with our present Pd data reveals that the essentially linear relation between hydrogen sensitivity and spectral LSPR position in the non-hydrogenated state indeed persists also in the near-infrared (NIR) spectral range, irrespective of not only particle size but also particle shape (Figure 7b). Interestingly, this consistent trend is strongly reminiscent of the well-established scaling of the bulk refractive index sensitivity of plasmonic nanoparticles with their size and shape, where the highest bulk refractive index sensitivity is achieved by shifting the LSPR to the NIR regime.[62,63] We highlight this point because in the present case we are altering the permittivity of the *particle itself via* hydrogen sorption and not the permittivity of the particle surroundings as in the case of plasmonic bulk refractive index sensing.

Finally, we note that in our experiments, Ar has been used as carrier gas due to its inertness. From an application perspective, it is motivating to briefly discuss the implications of also having oxygen present in the gas feed, as for example in air. The exposure of Pd or Pd alloys to oxygen might lead to formation of a surface oxide, which, upon contact with reducing species such as hydrogen, will be readily reduced even at ambient conditions. Hence we expect that the presence of oxygen would not affect the main findings of this work. From a more applied sensor-design perspective, it may imply that protective measures like applying a polymer coating[65] are necessary to prevent Pd oxidation and deactivation (by species such as CO).

DOI: 10.1021/acsnano.8b02835
ACS Nano 2018, 12, 9903−9912

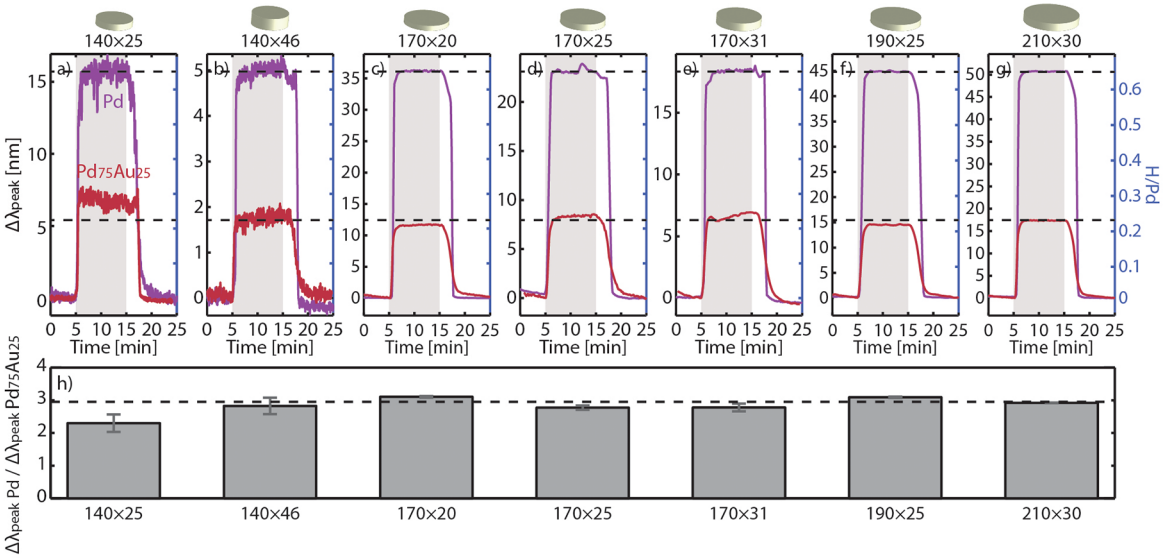

Figure 6. Nanoparticle size/volume dependence of $\Delta\lambda_{peak}$ obtained from LSPR measurements in transmission mode. The $\Delta\lambda_{peak}$ obtained at 250 mbar hydrogen partial pressure for differently sized Pd (purple) and $Pd_{75}Au_{25}$ (red) nanoparticles ((a) 140 × 25, (b) 140 × 46, (c) 170 × 20, (d) 170 × 25, (e) 170 × 31, (f) 190 × 25, and (g) 210 × 30, the first and the second number denote diameter and height in nm, respectively), are plotted in such a way that they are scaled to the hydrogen concentration (right *y*-axis shown in panel (g)) of Pd, *i.e.*, [H/Pd] = 0.65 (*cf.* Figure 3), as marked by the top black dashed line. Clearly, while the absolute $\Delta\lambda_{peak}$ varies significantly for each nanoparticle dimension (note the different scales of the *y*-axes in panels (a−g), the scaled $\Delta\lambda_{peak}$ of $Pd_{75}Au_{25}$ and Pd are very similar and in excellent agreement with the hydrogen content of 0.22 for $Pd_{75}Au_{25}$ (cf. Figure 3), marked by the bottom dashed line. The schematics of the nanoparticle drawn above each panel (a−g) show their relative sizes. Shaded areas denote hydrogen exposure to 250 mbar. (h) $\Delta\lambda_{peak}$ ratio of Pd to $Pd_{75}Au_{25}$, which agree very well with their H/Pd ratio of 0.65/0.22 = 2.95, marked with the dashed line. Error bars depict the variation in the ratio introduced by the noise and signal fluctuation during the hydrogenation step.

CONCLUSIONS

In summary, we have shown that (i) the amplitude of the plasmonic optical response of hydride-forming Pd or Pd alloy nanoparticles to hydrogen (*i.e.*, the sensitivity defined as $\Delta\lambda_{peak}$/[H/Pd]) is defined solely by the spectral LSPR position of the nanoparticles in the non-hydrogenated state and can be maximized by red-shifting the LSPR into the NIR spectral range, and (ii) to a first approximation the amplitude of the plasmonic optical response is constant and independent from the composition of the alloy (at least up to 25 at. % as demonstrated here) for particles of similar dimension. These findings can be interpreted as universal design rules for metal-hydride-based plasmonic hydrogen sensors and are thus of central importance for their further optimization and for their integration in real devices, as they not only enable the rational design and sensitivity optimization of suitable nanostructures but also provide the necessary fundamental understanding of their intrinsic limitations. Furthermore, our theoretical analysis indicates that the design rules found are expected to be applicable not only to any H/Pd/metal combination, provided that the metal does not interact strongly with hydrogen (*e.g.*, Ag), as we specifically demonstrate here for the H/Pd/Au and H/Pd/Cu systems. Hence, our main findings also shed light on generic fundamental materials science aspects of optical properties of alloy nanomaterials in general. From an alternative sensor perspective, establishing the nature of the scaling between plasmonic response and hydrogen concentration in nanoalloys will enable the use of the powerful single nanoparticle experimental techniques *in situ* EELS[7,29,30] and plasmonic nanospectroscopy[5,6,9,31,32] to generate deeper insights into the fundamentals of the metal−hydrogen interactions of complex materials at the individual nanoparticle level.

In a wider perspective, the hydride formation in metals in general and metal alloys in particular is of interest in the context of studies related to hydrogen strorage,[66] solute−solute interactions,[67] systems with reduced dimensions and modulated hydrogen affinity,[68,69] as well as defects in solids,[70] and also in other more specific context, *e.g.*, for the tunneling mechanism of diffusion of atoms in solids.[71] Therefore, we predict that our key results and the demonstrated experimental approach will find application beyond hydrogen sensing. Furthermore, combining the QCM with nanoplasmonic sensing is possible in both liquid and gaseous environments and will thus enable studies of processes like nanostructure oxidation or corrosion, as well as intercalation.

METHODS

Alloy Nanoparticle Fabrication. Both samples on QCM crystals (Laptech, SC-cut, 10 MHz fundamental frequency) and glass substrates (Borofloat, Schott Scandinavia AB) were fabricated by following procedures detailed elsewhere[13,40] based on layer by layer deposition through a mask and subsequent thermal annealing. For QCM crystals, a 1 nm Cr adhesion layer (Lesker PVD 225 evaporator, base pressure of 5×10^{-7} Torr, evaporation rate 1 Å s^{-1}) and 100 nm SiO_2 (PECVD, STS) were subsequently deposited, prior to nanoparticles fabrication. The alloying step was carried out at 400 °C by annealing for 72 h 4% H_2 in Ar.

Simultaneous QCM and LSPR Measurement. The QCM window-module (chamber volume *ca.* 40 μL, QSense Explorer window module, Biolin Scientific AB) was connected to a series of mass flow controllers (Bronkhorst ΔP) to regulate the H_2 partial pressure in Ar carrier gas at a constant total flow rate of 75 mL min^{-1}. A bifurcated fiber optic reflectance probe (FCR-7UV400C-2-ME-HTX, Avantes) positioned above the window was connected to a light source (AvaLight-Hal-S, Avantes) and a fixed-grating spectrophotometer (AvaSpec HS-TEC, Avantes). Data collection for QCM and LSPR measurements was executed by QTools (Biolin Scientific AB)

DOI: 10.1021/acsnano.8b02835
ACS Nano 2018, 12, 9903−9912

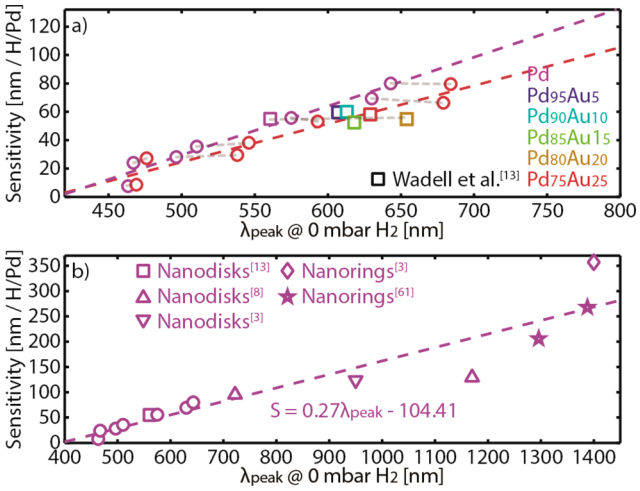

Figure 7. Universal optical response or "hydrogen sensitivity" curve for Pd and PdAu alloy nanoparticles. (a) The sensitivity factor [expressed as nm/[H/Pd] as a function of λ_{peak} in the non-hydrogenated state. It reveals a universal linear dependence of the sensitivity (purple and red dashed lines, regressed to Pd and $Pd_{75}Au_{25}$ data points, respectively) on the spectral position of the LSPR of the nanoparticles in the non-hydrogenated state. Furthermore, the data again illustrate that for alloyed nanoparticles with similar dimension the amplitude of the optical response is essentially constant irrespective of composition; see Pd and $Pd_{75}Au_{25}$ data pairs (connected with gray dashed lines) and the data set adapted from Wadell et al.[13] (squares). The points depicted as circles correspond to the data shown in Figure 6. (b) A plot of the sensitivity factor as a function of λ_{peak} in the non-hydrogenated state for pure Pd nanoparticles of a wide range of sizes and two different shapes (nanodisks and nanorings), constructed based on the results generated in the present study, as well as literature data obtained at similar conditions. The plot clearly reveals that the essentially linear relation between amplitude of optical response to hydrogen and spectral LSPR position in the non-hydrogenated state persists also in the NIR spectral range, irrespective of not only of particle size but also particle shape.

and Insplorer (Insplorion AB) softwares, respectively. A photograph of the experimental setup is shown in SI, Figure S1. Prior to measurements, the samples are subjected to 10 cycles of alternating 10 min flushes of Ar and 25% H_2. All measurements were performed at 303 K.

LSPR Measurement on Glass Samples. The samples were mounted in a quartz tube gas flow reactor system with optical access (Insplorion X1, Insplorion AB),[72] connected to a series of flow controllers (Bronkhorst ΔP) regulating the H_2 partial pressure in the Ar carrier gas, with a total flow rate of 100 mL min^{-1}. Optical transmission measurements were done via a fiber coupled halogen lamp (AvaLight-Hal-S, Avantes) and a fixed grating spectrophotometer (AvaSpec-1024, Avantes). For the 140 nm × 25 nm and 140 nm × 46 nm samples, an AvaSpec HS-TEC spectrophotometer, which enabled better resolution in the spectral range of 350−450 nm, was used instead. Data collection was carried out using the Insplorer software (Insplorion AB). Prior to measurements, the samples are subjected to 10 cycles of alternating 10 min flushes of Ar and 25% H_2. All measurements were performed at 303 K.

ASSOCIATED CONTENT

Supporting Information

The Supporting Information is available free of charge on the ACS Publications website at DOI: 10.1021/acsnano.8b02835.

Experimental setup and protocol, blank QCM crystal reference and data correction, calculation of hydrogen concentration from QCM signal, nanoparticle size distribution, Au nanoparticles control measurements, hydrogen concentration in the α-phase, fwhm-to-hydrogen concentration correlation, extinction-to-hydrogen concentration correlation, optical extinction spectra of Pd and PdAu nanoparticles on QCM crystals, optical extinction spectra of Pd and $Pd_{75}Au_{25}$ nanoparticles on glass samples, optical property analysis based on the Drude model, optical signal−hydrogen concentration correlation in PdCu alloy nanoparticles (PDF)

AUTHOR INFORMATION

Corresponding Authors

*(C.L.) clangham@chalmers.se

*(F.A.A.N.) ferryn@chalmers.se

ORCID

Ferry Anggoro Ardy Nugroho: 0000-0001-5571-0454

Christoph Langhammer: 0000-0003-2180-1379

Notes

The authors declare no competing financial interest.

ACKNOWLEDGMENTS

We acknowledge financial support from the Swedish Foundation for Strategic Research Framework project RMA15-0052, the Knut and Alice Wallenberg Foundation project 2016.0210, and the Chalmers Area of Advance for Nanoscience and Nanotechnology. We also thank the Knut and Alice Wallenberg Foundation for their support of the infrastructure in the MC2 nanofabrication laboratory at Chalmers. V.P.Z. acknowledges support of the Russian Federal Agency for Scientific Organizations (project 0303-2016-0001). F.A.A.N. thanks Prof. Yudhie Andriyana (Padjadjaran University) for the discussions on the statistics.

REFERENCES

(1) Wadell, C.; Syrenova, S.; Langhammer, C. Plasmonic Hydrogen Sensing with Nanostructured Metal Hydrides. *ACS Nano* **2014**, *8*, 11925−11940.

(2) Langhammer, C.; Zhdanov, V. P.; Zorić, I.; Kasemo, B. Size-Dependent Kinetics of Hydriding and Dehydriding of Pd Nanoparticles. *Phys. Rev. Lett.* **2010**, *104*, 135502.

(3) Zorić, I.; Larsson, E. M.; Kasemo, B.; Langhammer, C. Localized Surface Plasmons Shed Light on Nanoscale Metal Hydrides. *Adv. Mater.* **2010**, *22*, 4628−4633.

(4) Wadell, C.; Pingel, T.; Olsson, E.; Zorić, I.; Zhdanov, V. P.; Langhammer, C. Thermodynamics of Hydride Formation and Decomposition in Supported Sub-10nm Pd Nanoparticles of Different Sizes. *Chem. Phys. Lett.* **2014**, *603*, 75−81.

(5) Syrenova, S.; Wadell, C.; Nugroho, F. A. A.; Gschneidtner, T. A.; Diaz Fernandez, Y. A.; Nalin, G.; Świtlik, D.; Westerlund, F.; Antosiewicz, T. J.; Zhdanov, V. P.; Moth-Poulsen, K.; Langhammer, C. Hydride Formation Thermodynamics and Hysteresis in Individual Pd Nanocrystals with Different Size and Shape. *Nat. Mater.* **2015**, *14*, 1236−1244.

(6) Alekseeva, S.; Bastos da Silva Fanta, A.; Iandolo, B.; Antosiewicz, T. J.; Nugroho, F. A. A.; Wagner, J. B.; Burrows, A.; Zhdanov, V. P.; Langhammer, C. Grain Boundary Mediated Hydriding Phase Transformations in Individual Polycrystalline Metal Nanoparticles. *Nat. Commun.* **2017**, *8*, 1084.

(7) Baldi, A.; Narayan, T. C.; Koh, A. L.; Dionne, J. A. *In Situ* Detection of Hydrogen-Induced Phase Transitions in Individual Palladium Nanocrystals. *Nat. Mater.* **2014**, *13*, 1143−1148.

DOI: 10.1021/acsnano.8b02835
ACS Nano 2018, 12, 9903−9912

(8) Langhammer, C.; Zorić, I.; Kasemo, B.; Clemens, B. M. Hydrogen Storage in Pd Nanodisks Characterized with a Novel Nanoplasmonic Sensing Scheme. *Nano Lett.* **2007**, *7*, 3122−3127.
(9) Liu, N.; Tang, M. L.; Hentschel, M.; Giessen, H.; Alivisatos, A. P. Nanoantenna-Enhanced Gas Sensing in a Single Tailored Nanofocus. *Nat. Mater.* **2011**, *10*, 631−636.
(10) Langhammer, C.; Larsson, E. M.; Kasemo, B.; Zorić, I. Indirect Nanoplasmonic Sensing: Ultrasensitive Experimental Platform for Nanomaterials Science and Optical Nanocalorimetry. *Nano Lett.* **2010**, *10*, 3529−3538.
(11) Tittl, A.; Mai, P.; Taubert, R.; Dregely, D.; Liu, N.; Giessen, H. Palladium-Based Plasmonic Perfect Absorber in the Visible Wavelength Range and Its Application to Hydrogen Sensing. *Nano Lett.* **2011**, *11*, 4366−4369.
(12) Chiu, C.-Y.; Huang, M. H. Polyhedral Au-Pd Core-Shell Nanocrystals as Highly Spectrally Responsive and Reusable Hydrogen Sensors in Aqueous Solution. *Angew. Chem., Int. Ed.* **2013**, *52*, 12709−12713.
(13) Wadell, C.; Nugroho, F. A. A.; Lidström, E.; Iandolo, B.; Wagner, J. B.; Langhammer, C. Hysteresis-Free Nanoplasmonic Pd-Au Alloy Hydrogen Sensors. *Nano Lett.* **2015**, *15*, 3563−3570.
(14) Matuschek, M.; Singh, D. P.; Jeong, H. H.; Nesterov, M.; Weiss, T.; Fischer, P.; Neubrech, F.; Liu, N. Chiral Plasmonic Hydrogen Sensors. *Small* **2018**, *14*, 1702990.
(15) Poyli, M. A.; Silkin, V. M.; Chernov, I. P.; Echenique, P. M.; Muiño, R. D.; Aizpurua, J. Multiscale Theoretical Modeling of Plasmonic Sensing of Hydrogen Uptake in Palladium Nanodisks. *J. Phys. Chem. Lett.* **2012**, *3*, 2556−2561.
(16) Strohfeldt, N.; Tittl, A.; Schäferling, M.; Neubrech, F.; Kreibig, U.; Griessen, R.; Giessen, H. Yttrium Hydride Nanoantennas for Active Plasmonics. *Nano Lett.* **2014**, *14*, 1140−1147.
(17) Sterl, F.; Strohfeldt, N.; Walter, R.; Griessen, R.; Tittl, A.; Giessen, H. Magnesium as Novel Material for Active Plasmonics in the Visible Wavelength Range. *Nano Lett.* **2015**, *15*, 7949−7955.
(18) Boelsma, C.; Bannenberg, L. J.; van Setten, M. J.; Steinke, N.-J.; van Well, A. A.; Dam, B. Hafnium—an Optical Hydrogen Sensor Spanning Six Orders in Pressure. *Nat. Commun.* **2017**, *8*, 15718.
(19) Gremaud, R.; Broedersz, C. P.; Borsa, D. M.; Borgschulte, A.; Mauron, P.; Schreuders, H.; Rector, J. H.; Dam, B.; Griessen, R. Hydrogenography: An Optical Combinatorial Method To Find New Light-Weight Hydrogen-Storage Materials. *Adv. Mater.* **2007**, *19*, 2813−2817.
(20) Borsa, D. M.; Gremaud, R.; Baldi, A.; Schreuders, H.; Rector, J. H.; Kooi, B.; Vermeulen, P.; Notten, P. H. L.; Dam, B.; Griessen, R. Structural, Optical, and Electrical Properties of Mg y Ti 1 − y H x Thin Films. *Phys. Rev. B: Condens. Matter Mater. Phys.* **2007**, *75*, 205408.
(21) Ludwig, A.; Cao, J.; Dam, B.; Gremaud, R. Opto-Mechanical Characterization of Hydrogen Storage Properties of Mg−Ni Thin Film Composition Spreads. *Appl. Surf. Sci.* **2007**, *254*, 682−686.
(22) Baldi, A.; Pálsson, G. K.; Gonzalez-Silveira, M.; Schreuders, H.; Slaman, M.; Rector, J. H.; Krishnan, G.; Kooi, B. J.; Walker, G. S.; Fay, M. W.; Hjörvarsson, B.; Wijngaarden, R. J.; Dam, B.; Griessen, R. Mg/Ti Multilayers: Structural and Hydrogen Absorption Properties. *Phys. Rev. B: Condens. Matter Mater. Phys.* **2010**, *81*, 224203.
(23) Huiberts, J. N.; Griessen, R.; Rector, J. H.; Wijngaarden, R. J.; Dekker, J. P.; de Groot, D. G.; Koeman, N. J. Yttrium and Lanthanum Hydride Films with Switchable Optical Properties. *Nature* **1996**, *380*, 231−234.
(24) Yoshimura, K.; Yamada, Y.; Okada, M. Optical Switching of Mg-Rich Mg−Ni Alloy Thin Films. *Appl. Phys. Lett.* **2002**, *81*, 4709−4711.
(25) Ngene, P.; Radeva, T.; Slaman, M.; Westerwaal, R. J.; Schreuders, H.; Dam, B. Seeing Hydrogen in Colors: Low-Cost and Highly Sensitive Eye Readable Hydrogen Detectors. *Adv. Funct. Mater.* **2014**, *24*, 2374−2382.
(26) Radeva, T.; Ngene, P.; Slaman, M.; Westerwaal, R.; Schreuders, H.; Dam, B. Highly Sensitive and Selective Visual Hydrogen Detectors Based on YxMg1−x Thin Films. *Sens. Actuators, B* **2014**, *203*, 745−751.
(27) Isaac, N. A.; Ngene, P.; Westerwaal, R. J.; Gaury, J.; Dam, B.; Schmidt-Ott, A.; Biskos, G. Optical Hydrogen Sensing with Nanoparticulate Pd−Au Films Produced by Spark Ablation. *Sens. Actuators, B* **2015**, *221*, 290−296.
(28) Pivak, Y.; Gremaud, R.; Gross, K.; Gonzalez-Silveira, M.; Walton, A.; Book, D.; Schreuders, H.; Dam, B.; Griessen, R. Effect of the Substrate on the Thermodynamic Properties of PdHx Films Studied by Hydrogenography. *Scr. Mater.* **2009**, *60*, 348−351.
(29) Narayan, T. C.; Baldi, A.; Koh, A. L.; Sinclair, R.; Dionne, J. A. Reconstructing Solute-Induced Phase Transformations within Individual Nanocrystals. *Nat. Mater.* **2016**, *15*, 768−774.
(30) Narayan, T. C.; Hayee, F.; Baldi, A.; Leen Koh, A.; Sinclair, R.; Dionne, J. A. Direct Visualization of Hydrogen Absorption Dynamics in Individual Palladium Nanoparticles. *Nat. Commun.* **2017**, *8*, 14020.
(31) Shegai, T.; Langhammer, C. Hydride Formation in Single Palladium and Magnesium Nanoparticles Studied by Nanoplasmonic Dark-Field Scattering Spectroscopy. *Adv. Mater.* **2011**, *23*, 4409−4414.
(32) Tang, M. L.; Liu, N.; Dionne, J. A.; Alivisatos, A. P. Observations of Shape-Dependent Hydrogen Uptake Trajectories from Single Nanocrystals. *J. Am. Chem. Soc.* **2011**, *133*, 13220−13223.
(33) Larsson, E. M.; Edvardsson, M. E. M.; Langhammer, C.; Zorić, I.; Kasemo, B. A Combined Nanoplasmonic and Electrodeless Quartz Crystal Microbalance Setup. *Rev. Sci. Instrum.* **2009**, *80*, 125105.
(34) Rydén, J.; Hjörvarsson, B.; Ericsson, T.; Karlsson, E.; Krozer, A.; Kasemo, B. Unusual Kinetics of Hydride Formation in Mg-Pd Sandwiches, Studied by Hydrogen Profiling and Quartz Crystal Microbalance Measurements. *J. Less-Common Met.* **1989**, *152*, 295−309.
(35) Westerwaal, R. J.; Rooijmans, J. S. A.; Leclercq, L.; Gheorghe, D. G.; Radeva, T.; Mooij, L.; Mak, T.; Polak, L.; Slaman, M.; Dam, B.; et al. Nanostructured Pd−Au Based Fiber Optic Sensors for Probing Hydrogen Concentrations in Gas Mixtures. *Int. J. Hydrogen Energy* **2013**, *38*, 4201−4212.
(36) Opalka, S. M.; Huang, W.; Wang, D.; Flanagan, T. B.; Løvvik, O. M.; Emerson, S. C.; She, Y.; Vanderspurt, T. H. Hydrogen Interactions with the PdCu Ordered B2 Alloy. *J. Alloys Compd.* **2007**, *446-447*, 583−587.
(37) Galipaud, J.; Martin, M. H.; Roué, L.; Guay, D. Pulsed Laser Deposition of PdCuAu Alloy Membranes for Hydrogen Absorption Study. *J. Phys. Chem. C* **2015**, *119*, 26451−26458.
(38) Amandusson, H.; Ekedahl, L.-G.; Dannetun, H. Hydrogen Permeation through Surface Modified Pd and PdAg Membranes. *J. Membr. Sci.* **2001**, *193*, 35−47.
(39) Sonwane, C. G.; Wilcox, J.; Ma, Y. H. Achieving Optimum Hydrogen Permeability in PdAg and PdAu Alloys. *J. Chem. Phys.* **2006**, *125*, 184714.
(40) Nugroho, F. A. A.; Iandolo, B.; Wagner, J. B.; Langhammer, C. Bottom-Up Nanofabrication of Supported Noble Metal Alloy Nanoparticle Arrays for Plasmonics. *ACS Nano* **2016**, *10*, 2871−2879.
(41) Nayebossadri, S.; Speight, J. D.; Book, D. Pd−Cu−M (M = Y, Ti, Zr, V, Nb, and Ni) Alloys for the Hydrogen Separation Membrane. *ACS Appl. Mater. Interfaces* **2017**, *9*, 2650−2661.
(42) Luo, S.; Wang, D.; Flanagan, T. B. Thermodynamics of Hydrogen in Fcc *Pd−Au Alloys*. *J. Phys. Chem. B* **2010**, *114*, 6117−6125.
(43) Mock, J. J.; Hill, R. T.; Degiron, A.; Zauscher, S.; Chilkoti, A.; Smith, D. R. Distance-Dependent Plasmon Resonant Coupling between a Gold Nanoparticle and Gold Film. *Nano Lett.* **2008**, *8*, 2245−2252.
(44) Mubeen, S.; Zhang, S.; Kim, N.; Lee, S.; Krämer, S.; Xu, H.; Moskovits, M. Plasmonic Properties of Gold Nanoparticles Separated from a Gold Mirror by an Ultrathin Oxide. *Nano Lett.* **2012**, *12*, 2088−2094.
(45) Knight, M. W.; Wu, Y.; Lassiter, J. B.; Nordlander, P.; Halas, N. J. Substrates Matter: Influence of an Adjacent Dielectric on an Individual Plasmonic Nanoparticle. *Nano Lett.* **2009**, *9*, 2188−2192.

DOI: 10.1021/acsnano.8b02835
ACS Nano 2018, 12, 9903−9912

(46) Ding, T.; Mertens, J.; Sigle, D. O.; Baumberg, J. J. Capillary-Force-Assisted Optical Tuning of Coupled Plasmons. *Adv. Mater.* **2015**, *27*, 6457−6461.
(47) Jonsson, M. P.; Jönsson, P.; Höök, F. Simultaneous Nanoplasmonic and Quartz Crystal Microbalance Sensing: Analysis of Biomolecular Conformational Changes and Quantification of the Bound Molecular Mass. *Anal. Chem.* **2008**, *80*, 7988−7995.
(48) Zhu, J.; Huang, S.; Ye, J.; Zhang, X.; Liu, G. Design of a Quartz Crystal with Transparent Electrode Used for Both QCM-D and LSPR Technology. *Sens. Actuators, A* **2015**, *229*, 141−146.
(49) Fredriksson, H.; Alaverdyan, Y.; Dmitriev, A.; Langhammer, C.; Sutherland, D. S.; Zäch, M.; Kasemo, B. Hole−Mask Colloidal Lithography. *Adv. Mater.* **2007**, *19*, 4297−4302.
(50) Sauerbrey, G. Verwendung von Schwingquarzen Zur Wägung Dünner Schichten Und Zur Mikrowägung. *Eur. Phys. J. A* **1959**, *155*, 206−222.
(51) Rocklein, M. N.; George, S. M. Temperature-Induced Apparent Mass Changes Observed during Quartz Crystal Microbalance Measurements of Atomic Layer Deposition. *Anal. Chem.* **2003**, *75*, 4975−4982.
(52) Wicke, E.; Brodowsky, H.; Züchner, H. *Hydrogen in Palladium and Palladium Alloys*. Springer: Berlin, Heidelberg, 1978; pp 73−155.
(53) Frazier, G. A.; Glosser, R. Phase Diagrams of Thin Films of the Palladium Hydrogen System Using a Quartz Crystal Thickness Monitor. *J. Phys. D: Appl. Phys.* **1979**, *12*, L113−L115.
(54) Hubkowska, K.; Łukaszewski, M.; Czerwiński, A. Influence of Temperature on Hydrogen Electrosorption into Palladium−Noble Metal Alloys. Part 1: Palladium−Gold Alloys. *Electrochim. Acta* **2010**, *56*, 235−242.
(55) Nørskov, J. K.; Besenbacher, F. Theory of Hydrogen Interaction with Metals. *J. Less-Common Met.* **1987**, *130*, 475−490.
(56) Burlaka, V.; Wagner, S.; Hamm, M.; Pundt, A. Suppression of Phase Transformation in Nb−H Thin Films below Switchover Thickness. *Nano Lett.* **2016**, *16*, 6207−6212.
(57) Silkin, V. M.; Díez Muiño, R.; Chernov, I. P.; Chulkov, E. V.; Echenique, P. M. Tuning the Plasmon Energy of Palladium-Hydrogen Systems by Varying the Hydrogen Concentration. *J. Phys.: Condens. Matter* **2012**, *24*, 104021.
(58) Houari, A.; Matar, S. F.; Eyert, V. Electronic Structure and Crystal Phase Stability of Palladium Hydrides. *J. Appl. Phys.* **2014**, *116*, 173706.
(59) Methfessel, M.; Kubler, J. Bond Analysis of Heats of Formation: Application to Some Group VIII and IB Hydrides. *J. Phys. F: Met. Phys.* **1982**, *12*, 141−161.
(60) Ke, X.; Kramer, G. J.; Løvvik, O. M. The Influence of Electronic Structure on Hydrogen Absorption in Palladium Alloys. *J. Phys.: Condens. Matter* **2004**, *16*, 6267−6277.
(61) Burch, R.; Buss, R. G. Absorption of Hydrogen by Palladium−Copper Alloys. Part 1.—Experimental Measurements. *J. Chem. Soc., Faraday Trans. 1* **1975**, *71*, 913.
(62) Miller, M. M.; Lazarides, A. A. Sensitivity of Metal Nanoparticle Surface Plasmon Resonance to the Dielectric Environment. *J. Phys. Chem. B* **2005**, *109*, 21556−21565.
(63) Saison-Francioso, O.; Lévêque, G.; Boukherroub, R.; Szunerits, S.; Akjouj, A. Dependence between the Refractive-Index Sensitivity of Metallic Nanoparticles and the Spectral Position of Their Localized Surface Plasmon Band: A Numerical and Analytical Study. *J. Phys. Chem. C* **2015**, *119*, 28551−28559.
(64) Langhammer, C.; Larsson, E. M.; Zhdanov, V. P.; Zorić, I. Asymmetric Hysteresis in Nanoscopic Single-Metal Hydrides: Palladium Nanorings. *J. Phys. Chem. C* **2012**, *116*, 21201−21207.
(65) Ngene, P.; Westerwaal, R. J.; Sachdeva, S.; Haije, W.; de Smet, L. C. P. M.; Dam, B. Polymer-Induced Surface Modifications of Pd-Based Thin Films Leading to Improved Kinetics in Hydrogen Sensing and Energy Storage Applications. *Angew. Chem., Int. Ed.* **2014**, *53*, 12081−12085.
(66) Sakintuna, B.; Lamari-Darkrim, F.; Hirscher, M. Metal Hydride Materials for Solid Hydrogen Storage: A Review. *Int. J. Hydrogen Energy* **2007**, *32*, 1121−1140.
(67) Lacher, J. R. A. Theoretical Formula for the Solubility of Hydrogen in Palladium. *Proc. R. Soc. London, Ser. A* **1937**, *161*, 525−545.
(68) Steyrer, G.; Peisl, J. Coherent Phase Transition in NbH_x studied by Neutron Radiography. *Europhys. Lett.* **1986**, *2*, 835−841.
(69) Miceli, P. F.; Zabel, H.; Cunningham, J. E. Hydrogen-Induced Strain Modulation in Nb-Ta Superlattices. *Phys. Rev. Lett.* **1985**, *54*, 917−919.
(70) Kircheim, R.; Pundt, A. *Physical Metallurgy*, 5th ed.; Hono, K., Ed.; Elsevier, 2014.
(71) Alefeld, G.; Völkl, J. *Hydrogen in Metals I—Basic Properties*; Alefeld, G., Völkl, J., Eds.; Springer: Berlin, Heidelberg, 1978.
(72) Nugroho, F. A. A.; Diaz de Zerio Mendaza, A.; Lindqvist, C.; Antosiewicz, T. J.; Müller, C.; Langhammer, C. Plasmonic Nanospectroscopy for Thermal Analysis of Organic Semiconductor Thin Films. *Anal. Chem.* **2017**, *89*, 2575−2582.

DOI: 10.1021/acsnano.8b02835
ACS Nano 2018, 12, 9903−9912